



HAL
open science

Warming-induced monsoon precipitation phase change intensifies glacier mass loss in the southeastern Tibetan Plateau

Achille Jouberton, Thomas E. Shaw, Evan Miles, Michael Mccarthy, Stefan Fugger, Shaoting Ren, Amaury Dehecq, Wei Yang, Francesca Pellicciotti

► **To cite this version:**

Achille Jouberton, Thomas E. Shaw, Evan Miles, Michael Mccarthy, Stefan Fugger, et al.. Warming-induced monsoon precipitation phase change intensifies glacier mass loss in the southeastern Tibetan Plateau. *Proceedings of the National Academy of Sciences of the United States of America*, 2022, 119, 10.1073/pnas.2109796119 . insu-03859262

HAL Id: insu-03859262

<https://insu.hal.science/insu-03859262v1>


Submitted on 3 Jul 2024

HAL is a multi-disciplinary open access archive for the deposit and dissemination of scientific research documents, whether they are published or not. The documents may come from teaching and research institutions in France or abroad, or from public or private research centers.

L'archive ouverte pluridisciplinaire **HAL**, est destinée au dépôt et à la diffusion de documents scientifiques de niveau recherche, publiés ou non, émanant des établissements d'enseignement et de recherche français ou étrangers, des laboratoires publics ou privés.



Warming-induced monsoon precipitation phase change intensifies glacier mass loss in the southeastern Tibetan Plateau

Achille Jouberton^{a,b,1} , Thomas E. Shaw^a, Evan Miles^a , Michael McCarthy^{a,c} , Stefan Fugger^{a,b}, Shaoting Ren^{a,d}, Amaury Dehecq^{a,e,f} , Wei Yang^d, and Francesca Pellicciotti^{a,g} 

Edited by Michael Mann, The Pennsylvania State University, University Park, PA; received May 31, 2021; accepted July 20, 2022

Glaciers are key components of the mountain water towers of Asia and are vital for downstream domestic, agricultural, and industrial uses. The glacier mass loss rate over the southeastern Tibetan Plateau is among the highest in Asia and has accelerated in recent decades. This acceleration has been attributed to increased warming, but the mechanisms behind these glaciers' high sensitivity to warming remain unclear, while the influence of changes in precipitation over the past decades is poorly quantified. Here, we reconstruct glacier mass changes and catchment runoff since 1975 at a benchmark glacier, Parlung No. 4, to shed light on the drivers of recent mass losses for the monsoonal, spring-accumulation glaciers of the Tibetan Plateau. Our modeling demonstrates how a temperature increase (mean of $0.39\text{ }^{\circ}\text{C}\cdot\text{dec}^{-1}$ since 1990) has accelerated mass loss rates by altering both the ablation and accumulation regimes in a complex manner. The majority of the post-2000 mass loss occurred during the monsoon months, caused by simultaneous decreases in the solid precipitation ratio (from 0.70 to 0.56) and precipitation amount (-10%), leading to reduced monsoon accumulation (-26%). Higher solid precipitation in spring ($+18\%$) during the last two decades was increasingly important in mitigating glacier mass loss by providing mass to the glacier and protecting it from melting in the early monsoon. With bare ice exposed to warmer temperatures for longer periods, icemelt and catchment discharge have unsustainably intensified since the start of the 21st century, raising concerns for long-term water supply and hazard occurrence in the region.

climate change | glaciers | hydrological modeling | precipitation phase change

High Mountain Asia (HMA) is commonly referred to as the “Third Pole,” as it hosts the largest reservoir of ice and snow outside of the polar regions (1), which is relied upon by more than one-fifth of the world's population for domestic and industrial purposes (2). The cryosphere of HMA is highly sensitive to climate change (3), and its changes will negatively affect more than 800 million people living in the downstream river basins (4), a significant proportion of which depend on snow and glacier melt for their livelihoods (5) or are vulnerable to disasters related to melting glaciers such as glacial lake outburst floods (6). Glaciers of HMA have experienced contrasting mass changes that can be attributed to regional atmospheric circulation patterns (7, 8), sensitivity to warming climate (3, 9, 10), and changing seasonality and intensity of the summer monsoon (11–13). Glacier mass balances derived from field measurements and remote sensing reveal some of the greatest mass losses in the southeastern Tibetan Plateau (TP) (9, 14–16) (Fig. 1), where mass loss has accelerated over the past four decades (16–18). Glaciers of this region are commonly referred to as spring accumulation type (19, 20), or “maritime” glaciers (21) with large accumulation and coincident strong ablation that lead to high rates of mass turnover. Recent studies have found that these glaciers have a higher sensitivity to a change in temperature than to a change in precipitation (10, 19, 22), through its control on the ratio of snowfall to precipitation and melt energy during the ablation season. Notwithstanding their important insights, these results were mostly derived by artificially perturbing the temperature forcing by a fixed amount and analyzing the effects on the glacier-mass balance, and no study to date has been able to reconstruct more than three decades of real changes and chart the actual acceleration in glacier mass losses and impacts on runoff. The interplay and relative importance of the mechanisms explaining the mass loss acceleration thus remain unclear, especially over longer time periods. Moreover, most studies focus on glaciers and not the resulting catchment hydrological response, which remains unconstrained and yet crucial to understanding how ice reserves feed downstream water resources (23).

The application of glacio-hydrological models is crucial to understanding the links between past climate dynamics, observed mass change, and runoff (24) and can help bridge the gap between decadal mass changes observed with remote sensing and in situ data

Significance

Rapid mass loss of glaciers in High Mountain Asia has large consequences for downstream water supply and glacier-related hazards. Glaciers in the southeastern Tibetan Plateau are experiencing the highest mass loss rates within Asia, despite the limited impact of recent warming on their spring accumulation regime. Based on model simulations reconstructing the climate and glacier evolution of the last 45 y, we show that the recent acceleration in observed glacier mass loss was effected by a warming-induced shift from snowfall to rainfall during the monsoon months, exacerbated by decreasing monsoon precipitation since the 2000s and only partly mitigated by increasing spring precipitation. Our results reveal the processes behind the high sensitivity to climate warming for glaciers in this region.

Author contributions: A.J., T.E.S., E.M., M.M., S.F., and F.P. designed research; A.J. and T.E.S. performed research; A.J., T.E.S., S.R., A.D., and W.Y. analyzed data; A.J., T.E.S., E.M., and F.P. wrote the paper; M.M., S.R., and A.D. processed remote-sensing data; M.M., S.F., and A.D. provided inputs to the paper writing; and W.Y. provided in situ meteorological data.

The authors declare no competing interest.

This article is a PNAS Direct Submission.

Copyright © 2022 the Author(s). Published by PNAS. This article is distributed under [Creative Commons Attribution-NonCommercial-NoDerivatives License 4.0 \(CC BY-NC-ND\)](https://creativecommons.org/licenses/by-nc-nd/4.0/).

¹To whom correspondence may be addressed. Email: achille.jouberton@wsl.ch.

This article contains supporting information online at <https://www.pnas.org/lookup/suppl/doi:10.1073/pnas.2109796119/-DCSupplemental>.

Published September 6, 2022.

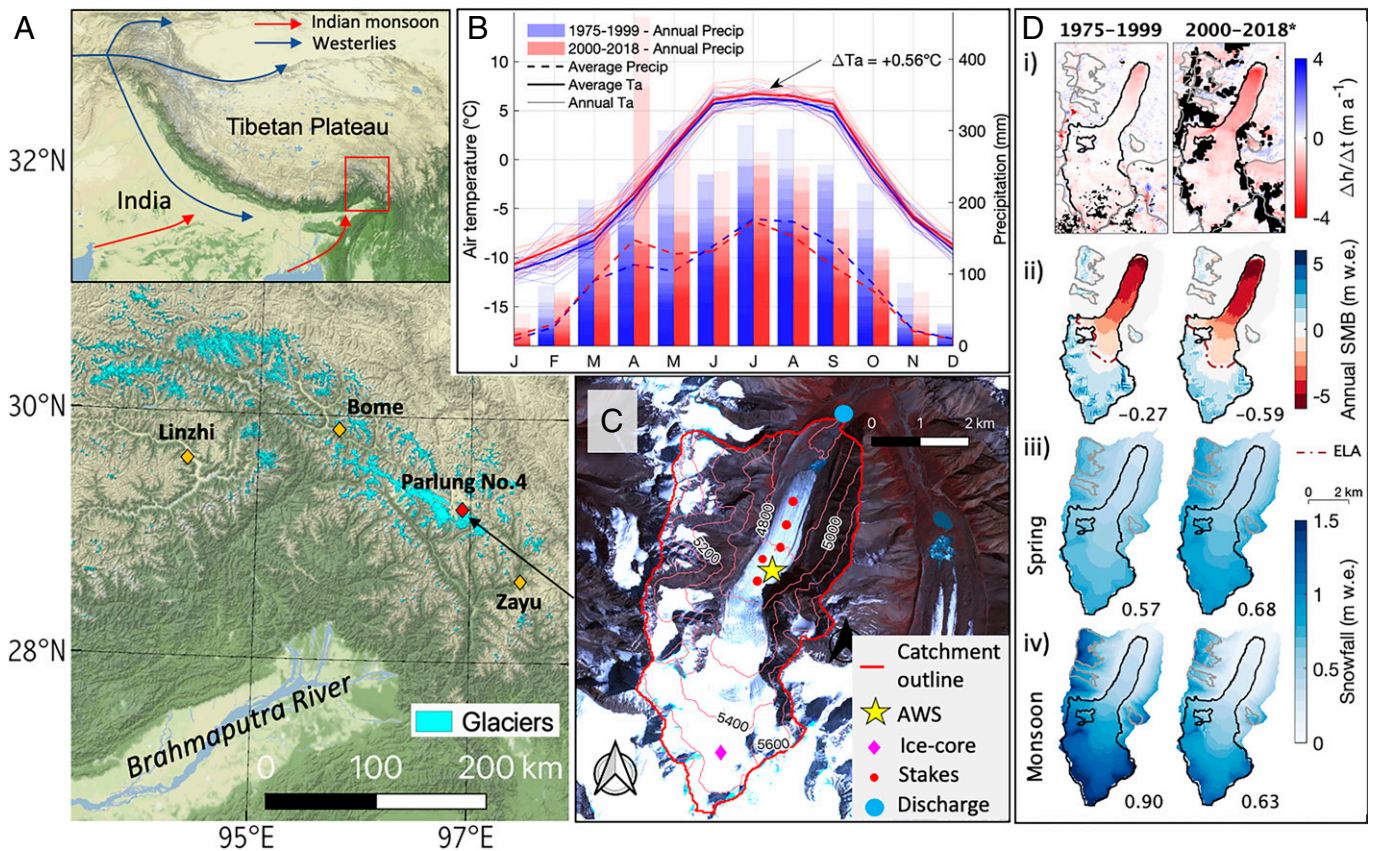


Fig. 1. Study catchment, its climate, and glacier mass changes since 1975. (A) Location of the study site in the southeastern part of the Tibetan Plateau and of the Zayu national weather station used for climate reconstruction. (B) Mean monthly temperature and precipitation reconstructed at the study site (4,600 m a.s.l.) for each individual year. The thick solid and dashed (blue and red) lines are the temperature and precipitation period average, respectively (1975 to 1999 and 2000 to 2018). (C) Study catchment and position of the main monitoring instruments. Another AWS is located 5 km north of the glacier terminus. (D) Comparison between the early and recent period for i) elevation change derived from DEM differencing, ii) simulated glacier surface mass balance (SMB), iii) simulated snowfall in spring, and iv) simulated snowfall during the monsoon. The outlines of Parlung No. 4 Glacier are shown in black, and the outlines of the surrounding glaciers are shown in gray. *Top Right elevation change map corresponds to the 2000 to 2014 period (the GMB is similar for the 2000 to 2018 period; cf. *SI Appendix*).

over an ablation season, while providing key insights into the past and future catchment hydrology. Such distributed models have been successfully applied at the catchment scale in Nepal (25, 26), in the Central TP (27), and in northwest China (28), but none have yet focused on the southeastern TP, a hotspot of negative mass balance. Such studies remain challenging because of a lack of representative data to calibrate and validate models, which can be difficult and costly to obtain, especially at higher elevations.

Here, we conduct a multidecadal glacio-hydrological study using a fully distributed model (TOPKAPI-ETH) for glacier mass balance (GMB) and runoff simulation at the Parlung No. 4 catchment in the southeastern TP. Parlung No. 4 Glacier (Fig. 1 A and C) is considered a benchmark glacier in this region, since its meteorology, surface energy fluxes, and mass balance have each been examined in recent years (19, 22) (more details in *SI Appendix*). The climate of the region is influenced by a southern westerlies trough and the Bay of Bengal monsoon vortex during spring and by the Indian monsoon in summer, exhibiting a double-peak precipitation pattern (Fig. 1B). We force the model with the best combination of local weather stations and bias-corrected reanalysis datasets (ERA5-Land and China meteorological forcing dataset [CMFD]) to reconstruct meteorological time series at an hourly resolution from 1975 to 2018. We then systematically calibrate and validate the model using in situ measurements including on- and off-glacier automatic weather stations (AWSs), ablation stakes, and proglacial discharge records, as well as remote-sensing observations of multidecadal glacier thinning and snow cover from Moderate Resolution Imaging Spectroradiometer (MODIS).

We use the model to investigate the reasons behind the acceleration in glacier mass loss and the consequences for catchment hydrology, and elucidate the mechanisms that make this region's glaciers so highly sensitive to a changing climate. For this, we analyze the changes in the solid water balance (ice and snow) within the glacier outlines, hereafter referred to as the "cryospheric water balance", which decreases with the melting of snow and ice and increases through solid precipitation input. We additionally examine the influence of changes in the meteorological forcing on the accumulation and ablation regimes. This permits an assessment of the key drivers and underlying processes that explain the changes in GMB since the 1970s. We divide the study period between an "early" (1975 to 1999) and a "recent" (2000 to 2018) period, consistent with most available geodetic observations in the region. We define spring and monsoon as the periods spanning from 1 March to 28 May and from 29 May to 28 September, respectively, according to the 1979 to 2015 climatological monsoon onset and demise dates estimated at Parlung No. 4 (13).

Results

Multidecadal Catchment Hydrology and Glacier Mass Balance.

The Parlung catchment experienced a statistically significant warming of $0.23\text{ }^\circ\text{C}\cdot\text{dec}^{-1}$ over the simulation period (1975 to 2018), rising to $0.39\text{ }^\circ\text{C}\cdot\text{dec}^{-1}$ since the early 1990s (Fig. 2A and *SI Appendix*, Fig. S9). Between 1975 to 1999 and 2000 to 2018, the mean annual GMB decreased by 0.32 meters water

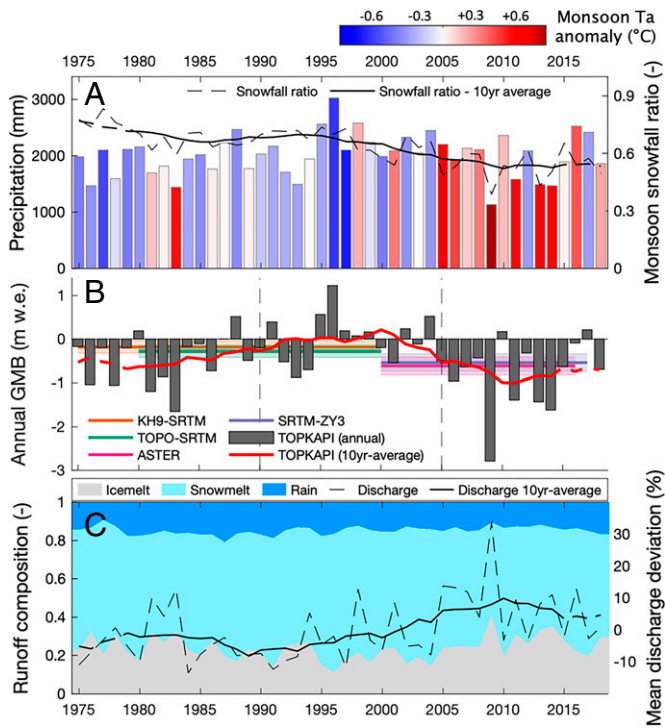


Fig. 2. Detailed history of the annual glacier-mass balance, catchment hydrology, and meteorology at Parlung No. 4 catchment. General trends are shown as moving averages calculated over a sliding window of 10 y (black solid lines). (A) Reconstructed climatic forcing averaged over the catchment area. The temperature indication (bar color) corresponds to the anomaly relative to the mean monsoon temperature of the whole period, and the snowfall to total precipitation ratio (black line) is averaged over the monsoon period. (B) Simulated and geodetic mass balance of Parlung No. 4 Glacier. The first and second vertical dashed lines indicate the start of the near-neutral GMB period and accelerated mass-loss period, respectively. KH9, KH9-Hexagon; SRTM, Shuttle Radar Topography Mission; TOPO, 1980 topographic maps; ASTER, Terra Advanced Spaceborne Thermal Emission and Reflection Radiometer; ZY3, Zi-Yuan 3. (C) Mean annual runoff composition (shaded area) and total catchment discharge deviation from the period average (black line).

equivalent. (from -0.27 to -0.59 m w.e.), concomitant with a warmer average catchment temperature ($+0.56$ °C, Fig. 1B), a decrease in the ratio of monsoon snowfall to monsoon total precipitation (hereafter, “monsoon snowfall ratio”) from 0.70 to 0.56 (Fig. 2A), a rise of the equilibrium line altitude (ELA) from 5,225 to 5,300 m above sea level (a.s.l.), and a 10% decrease in accumulation area (Fig. 1D). Changes in temperature and precipitation phase, combined with a decadal variability in total annual precipitation (SI Appendix, Fig. S9), led to a large interannual variability in GMB (Fig. 2B). Our simulations reveal that this broad acceleration of glacier mass was interrupted by a near-neutral annual GMB period in 1990 to 2004 ($+0.01$ m w.e.) that can be attributed to cooler temperatures and above-average monsoon precipitation, in agreement with similar findings at the nearby Parlung No. 94 Glacier (29); although it is not captured by the geodetic mass balance, owing to its coarse temporal resolution (Fig. 2B). From 2005 onward, the mean annual glacier mass loss intensified (to -0.79 m w.e.) and was accompanied by an increase in catchment runoff of 12% relative to 1975 to 1999 (Fig. 2C), mostly driven by an increase in icemelt ($+23\%$), whose contribution to runoff rose from 23 to 28%. Overall, 85% of the annual catchment discharge originated from meltwater since 2005, with the icemelt contribution rising as the monsoon progresses (SI Appendix, Fig. S29).

Changes in the Components of the Cryospheric Water Balance.

Changes in climate have resulted in both less mass input and more

mass loss, i.e., a decrease in solid precipitation and an increase in melt. The high mass turnover rate that is characteristic of the glaciers in the southeastern TP has amplified this phenomenon. The cryospheric water balance was more negative in the recent (2000 to 2018) period than in the early (1975 to 2000) period, with 307 mm w.e. of additional annual mass loss (Fig. 3B). The higher annual mass losses were caused by a decrease in solid precipitation (-163 mm w.e.) and an increase in icemelt ($+136$ mm w.e.) and snowmelt ($+8$ mm w.e.). While most of the changes in meltwater amount occurred during the monsoon, the reduction of annual solid precipitation masks a more complex seasonal pattern. Solid precipitation increased in spring ($+104$ mm w.e., Figs. 1D and 3B) but decreased by a larger amount during the monsoon (-249 mm w.e., Figs. 1D and 3B), especially in the accumulation area. While some of the reduced monsoon snowfall is due to the fact that monsoon precipitation amount decreased (-97 mm w.e.), we attributed a major portion of this reduction to a warming-induced change in precipitation phase from snowfall to rainfall (-152 mm w.e., corresponding to 50% of additional annual mass loss; cf. Fig. 3C and Materials and Methods for calculation details). The precipitation phase in spring was almost unaffected by this warming due to the persistence of negative absolute temperatures, resulting in a mean snowfall ratio decrease from 1 to 0.98. The increase in spring snowfall amount ($+18\%$) thus partially compensated for the reduced monsoon snowfalls (-26%), with its contribution to total annual snowfall rising from 32 to 41% between the early and the recent periods.

Attribution to the Specific Meteorological Changes. Over the last four decades, air temperature and precipitation have simultaneously varied, limiting the use of simple regression analyses (SI Appendix, Fig. S27) to estimate their relative influence on glacier mass balance. To disentangle the importance of each driver of glacier mass changes, we artificially set the spring and monsoon climate of the recent period to the mean conditions of the 1975 to 1989 period, before the start of the heightened warming trend (SI Appendix, Fig. S9). When the monsoon temperature is set to the mean 1975 to 1989 conditions, the annual GMB and catchment discharge during the recent period remained stable (Fig. 4A and B). This confirms that warmer monsoon temperatures are the main driver of accentuated mass loss and also of the recent catchment discharge increase. When the spring precipitation and monsoon precipitation are set to the mean 1975 to 1989 conditions, we find in both cases a more negative annual GMB during the 1990 to 2005 period, but from 2005 onward opposite and compensating effects are evident: The GMB is more negative for constant spring precipitation and less negative when the monsoon precipitation is maintained to its 1975 to 1989 baseline. This shows that the recent increase in spring precipitation counteracted the effect of decreasing monsoon precipitation on the post-2004 GMB, but did not mitigate the impact of temperature warming on the latter.

Fig. 4D–F shows the results of the forcing experiment described above at a daily time step for the year 2006, which experienced representative conditions of monsoon temperature and spring precipitation for the recent period (Fig. 4C). Under a scenario of colder monsoon temperatures (Fig. 4D), icemelt is reduced by 24% and snowfall by 4%, leading to an annual GMB less negative by 0.58 m w.e. When spring precipitation is reduced to its 1975 to 1989 baseline (Fig. 4E), the annual snowfall is reduced by 12% and the icemelt is increased by 16%, resulting in an annual GMB increase of 0.33 m w.e. Conversely, when monsoon precipitation is increased (Fig. 4F), the annual snowfall is increased by 2% and the icemelt reduced by 4%, leading to an

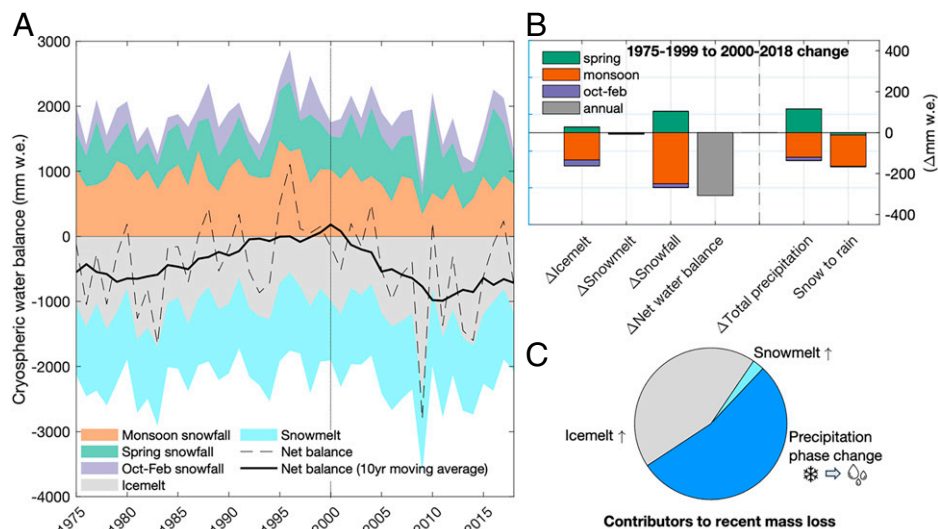


Fig. 3. Cryospheric water balance and contributors to recent mass loss. The net water balance is calculated as Snowfall – (Icemelt + Snowmelt). (A) Annual cryospheric water balance. (B) Changes in the cryospheric water balance between the early and the recent periods. A negative sign indicates less (more) water entering (leaving) the cryospheric storage. (C) Relative contribution of each component to the net annual mass loss over the glacier area. The change in snowfall was attributed to a change in precipitation phase and to a change in precipitation amounts; more details on this attribution are given in *Materials and Methods* as well as in *SI Appendix, Fig. S21*.

annual GMB less negative by 0.19 m w.e. Despite unperturbed air temperatures, changes in spring or monsoon snowfall produce a sizeable change in icemelt due to their control on snowpack presence and surface albedo (Fig. 4 E and F). Nevertheless, the monsoon temperature has a larger influence on the snowpack presence, and thus icemelt, compared with spring or monsoon precipitation, since it controls both snow accumulation and melt. The year 2009 experienced the most negative annual GMB (Fig. 2B) and is a very interesting case study (*SI Appendix, Fig. S26*), further confirming the predominant control of monsoon temperature on

GMB, with an artificial increase in monsoon precipitation unable to significantly offset the mass loss, owing to a low snowfall ratio (29%).

Discussion

Drivers behind Recent Acceleration in Glacier Mass Loss. We show how simultaneous changes in precipitation and temperature shape the GMB and catchment hydrology in the southeastern TP. At Parlung No. 4 the modification of the monsoon accumulation

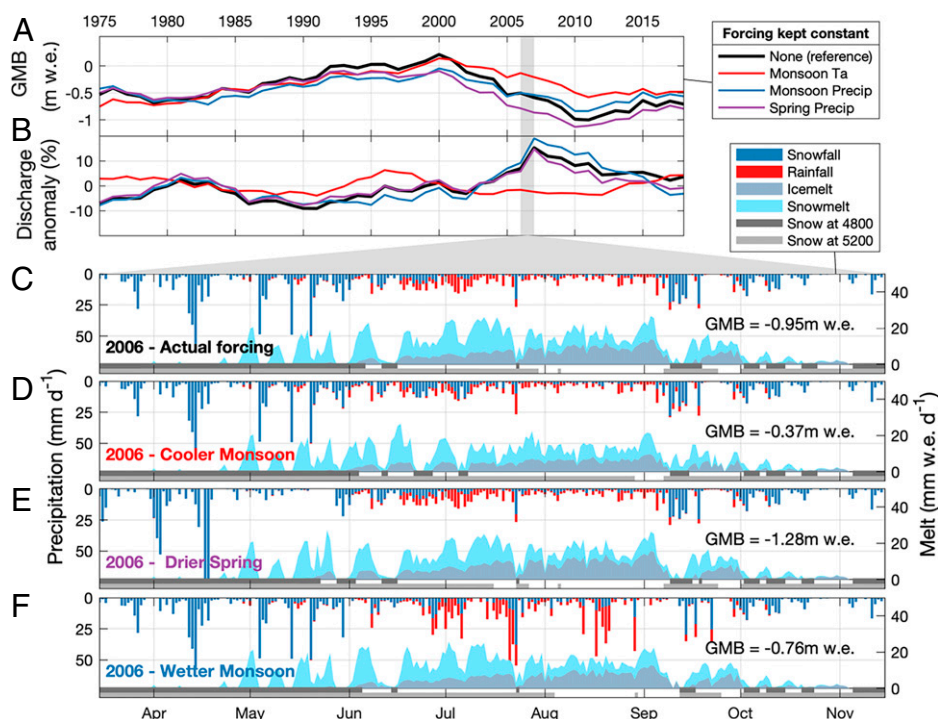


Fig. 4. Climatic forcings influence on the interannual variability of glacier-mass balance, melt amounts, and catchment discharge. (A and B) Annual glacier-mass balance (A) and annual mean catchment discharge (B) simulated when the respective meteorological variable is kept to its 1975 to 1989 level, compared with the reference run. (C–E) Example of the year 2006 and the changes in precipitation and melt amount, type, and timing when using the monsoon temperature (D), the spring precipitation (E), and the monsoon precipitation (F) of an average year of the 1975 to 1989 period. The melt and precipitation shown are catchment-wide average. The presence and absence of snow on the glacier at 4,800 m a.s.l. and 5,200 m a.s.l. are indicated by the bottom horizontal gray lines.

regime had a larger impact on the overall mass balance than the change in the ablation regime. The role of precipitation phase change in explaining those glaciers' sensitivity to future temperature change was suggested through sensitivity analyses (10, 22). Here we are able, through a comparison of the pre- and post-2000 cryospheric water balance, to demonstrate that those mechanisms were already at play in the past, by attributing the recent mass loss to this change in precipitation phase during the monsoon months (June to September) and to the concurrent icemelt intensification. Despite being commonly known as spring-accumulation-type glaciers (19), a large proportion of accumulation (50%) still occurs during the monsoon months, demonstrating a similarity with summer-accumulation-type glaciers, known for their high sensitivity to warming (30). Compared with summer-accumulation-type glaciers, principally located in the central TP and Himalayas (20), glaciers in the southeastern TP experience warmer summer temperatures and a relatively small annual temperature range, two factors leading to higher mass balance sensitivity with respect to air temperature (3) and explaining why they represent some of the largest mass losses in HMA. At Parlung No. 4, a warming of 0.56 °C from 1975 to 1999 to 2000 to 2018 has led to a decrease of mean annual mass balance of 0.32 m w.e. (from -0.27 to -0.59 m w.e.). Around half of the glaciers near to Parlung No. 4 have an area accumulation ratio of less than 20% (31). With temperatures increasing, the glacier areas receiving solid precipitation during the monsoon, already confined to the highest elevations, are shrinking.

Spring Precipitation Increasing, yet Insufficient. While the rise of monsoon temperature increases mass loss rates, especially due to its control on precipitation phase and melt rates, decadal changes in precipitation amounts can compensate for or accentuate these losses (Fig. 4). The role of spring accumulation and timing of monsoon onset has been shown to be crucial to the energy balance of TP glaciers, primarily through the control of surface albedo (7, 12). Here we show that due to a reduction in monsoon snowfalls, abundant spring snowfalls are increasingly important to reduce annual mass losses: They provide thicker snowpacks and augment albedo in the early monsoon season. Yet, this spring snowfall increase remains insufficient to compensate for the exacerbated losses caused by monsoon temperature and precipitation changes. Despite reports of a weakening of Indian summer monsoon in recent decades (32, 33) and evidence of increased spring precipitation attributed to an earlier onset of the South Asian summer monsoon (13, 34, 35), the mechanisms behind decadal changes in precipitation patterns are not yet fully understood. Several past studies have attempted to link moisture sources and glacier mass balance around the TP to large-scale teleconnection patterns (7, 26, 29, 36, 37) and revealed spatially variable controls and complex, locally occurring processes. Similar to a recent study focusing on a Nepalese glacier (26), we found no correlation between monsoon-related teleconnection indexes (El Niño–Southern Oscillation, Indian Ocean Dipole) and monsoon precipitation or annual glacier-mass balance at Parlung No. 4 Glacier (*SI Appendix, Table S3*). Mechanisms determining precipitation patterns (further discussed in *SI Appendix, section 7*) remain a future research direction as large uncertainty remains on how they might shape current and future changes in the high mountain cryosphere (38). With temperature expected to continue rising (39), projections show strong 21st century declines in snowfall (40), consequently driving severe reductions in snow retention (41), with implications for glacier mass loss and runoff.

Importance and Uncertainty of Precipitation Phase Change. Our modeling results show that precipitation phase change is a

major driver of glacier mass loss acceleration at Parlung No. 4. Analysis of glacier mass changes, hypsometry, and surface albedo within the southeastern TP indicates that Parlung No. 4 exhibits similar patterns to those of the surrounding region (*SI Appendix, section 1C*). Observations at regional meteorological stations cannot directly validate our precipitation phase change results, or demonstrate their relevance to the wider region, as they are all located at low elevations (all <4,300 m a.s.l.; *SI Appendix, Fig. S22*). However, regional trends in monsoon snowfall ratio derived from ERA5-Land indicate that this is a major process throughout this region (*SI Appendix, Fig. S24*). Additionally, considering the calibration and validation of TOPKAPI-ETH using a series of independent and process-specific datasets, the model's skills in reproducing snow processes lend high confidence to our findings (*SI Appendix, Figs. S15 and S19*). Nevertheless, our simulation-based results are subject to uncertainty related to meteorological forcing, model structure, and parameters (further discussed in *SI Appendix, section 6F*). To estimate uncertainty in precipitation phase changes, we performed Monte Carlo simulations by varying the key parameters controlling the precipitation quantity and phase partition. We thus ascribe an uncertainty to the modeled changes in annual average snowfall due to phase change: -152 ± 66 mm w.e. Despite this uncertainty, phase change remains a major driver of mass loss, accounting for $50 \pm 21\%$ of the recent acceleration in glacier mass loss. Our analysis showed that the uncertainty in phase changes increases with elevation (*SI Appendix, Fig. S22*). The application of fully distributed energy-balance models, including sublimation, refreezing, and more sophisticated precipitation partitioning schemes, could reduce those uncertainties, but would require robust meteorological forcing (42) and high-elevation evaluation data.

Implications for Water Supply and Melt-Related Disasters. We show that the acceleration in glacier mass loss was accompanied by an increase in catchment discharge due to enhanced icemelt. While this glacier showed a continuously negative mass balance over the last 15 y, it is unclear when its maximum runoff contribution (peak water) will be reached, and this remains a key direction of future research. The simulated increase in catchment discharge at the benchmark glacier Parlung No. 4 can serve as a reference for hydrological changes in the wider region of the southeastern TP (cf. *SI Appendix, section 1C* for details on the representativeness of Parlung No. 4). This unsustainable supply of water in the region (31) will, in the short to medium term, pave the way for the rapid formation and expansion of glacier lakes and their associated flood hazards (6, 43), but will also affect the seasonality and magnitude of catchment discharge in the longer term (4). Both hazards and changing water resources must be carefully considered for the future development of hydropower and water diversion projects planned in this region (44), while the consequences of the unsustainable flows of TP glaciers for ecosystems and other water uses remain largely unknown.

Materials and Methods

Glacio-Hydrological Model. We use TOPKAPI-ETH, a fully distributed, process-oriented, glacier-hydrological model (45, 46). We run the model at an hourly temporal resolution and with a 30-m grid resolution, from 1 January 1975 to 31 December 2018.

Meteorological Forcing Reconstruction. Several years of near-continuous hourly air temperature, precipitation, and shortwave radiation measured at an automatic weather station (AWSoff) located on a lateral moraine at 4,600 m

a.s.l., 5 km north of Parlung No. 4 Glacier, are used to correct reanalysis products and extrapolate national meteorological station data. We consider two reanalysis datasets: ERA5-Land, a replay of the land component of the ERA5 climate reanalysis with a finer spatial resolution (9 km) and covering the period 1981 to 2019 at hourly temporal resolution (47), and the CMFD, a fusion of ground-based observations with several gridded datasets from remote sensing and reanalysis (48), which has a temporal resolution of 3 h and a spatial resolution of 11 km and spans the period 1979 to 2018. We also consider the daily temperature and precipitation measured continuously since 1969 at Zayu's meteorological station, located 90 km southeast of Parlung No. 4. For each input variable, we select the dataset that reproduces best the AWSoff measurements (more details in *SI Appendix*). We use temperature measured at Zayu, disaggregated to hourly values (49), which we then extrapolate to AWSoff's location using monthly-hourly temperature lapse rates derived from overlapping measurement periods. We use the CMFD precipitation product, to which we apply a scaling factor (19) to correct the amount of annual precipitation, and use precipitation measured at Zayu to complete the four missing years (1975 to 1979). We compute hourly cloud cover transmissivity as the fraction of ERA5-Land incoming shortwave radiation divided by modeled potential, clear sky radiation (50).

Meteorological Forcing Distribution. We distribute the air temperature from the AWSoff location to each grid cell of the catchment using mean hourly-monthly lapse rates derived from temperature loggers installed at different elevations (4,600 to 5,100 m a.s.l.) during a 2018 to 2019 field campaign in Parlung region (51). Outside of summer months (i.e., October to May), some temperature loggers were very likely affected by snow coverage and we instead use mean monthly lapse rates available in the literature (52). Katabatic winds are common on Parlung No. 4 Glacier (51, 53), and the glacier cooling effect is considered by applying a temperature offset on the glacierized cells during above-freezing conditions, which we derived from the comparison of simultaneous on- and off-glacier temperature measurements (*SI Appendix*). Precipitation was similarly extrapolated, applying a constant in time, logarithmic vertical precipitation gradient. In the absence of measured precipitation gradients, we calibrate it against geodetic-mass balance (54) (*SI Appendix*). We use a constant temperature threshold of 2 °C to distinguish rainfall and snowfall. This was found in a previous study (55) to be the best value for Parlung Glacier when using a constant threshold to simulate total glacier melt in comparison with more sophisticated approaches using dynamic threshold temperatures (cf. *SI Appendix* for more details).

Snowmelt and Icemelt. TOPKAPI-ETH includes an enhanced temperature-index (ETI) model (56) that computes snow and ice surface melt at each grid cell based on the extrapolated air temperature and incoming shortwave radiation. Incoming shortwave radiation is computed in TOPKAPI-ETH from the sun position, cloud cover, topographic shading, and surface albedo, adjusted by the cloud cover transmissivity. Albedo is set to a maximum value after a snowfall event of a defined minimum magnitude, decreases linearly over time when temperature exceeds 0 °C, and falls to a constant lower value when bare ice is exposed (57).

Glacier Dynamics. Glacier flow needs to be considered when performing multidecadal glacier modeling, especially at Parlung No. 4 where it compensates 55% of surface ablation (58). TOPKAPI-ETH uses the delta-H flow parameterization (59) to redistribute the ice surface elevation change based on the simulated glacier-wide mass balance of that corresponding year. This parameterization of glacier geometry changes induced by flow was derived from DEMs (digital elevation models) differencing. The corresponding parameters were specifically derived from the observed 2000 to 2016 altitudinal thinning pattern (14) for Parlung No. 4 Glacier. The glacier dynamics algorithm is executed at the end of each hydrological year, when it also converts to ice the snow that has remained on the glacier for more than 1 y. Initial ice thickness was derived from the recent consensus estimate of ice-thickness distribution product (1) to which we added the elevation change derived from remote sensing during the period 1974 to 2000.

Geodetic Mass Balance. We use digital elevation models derived from remote-sensing observations as part of the calibration and validation procedure, with acquisition dates spanning from 1974 to 2017 (detailed inventory in

SI Appendix, Table S1). Digital elevation models were resampled to a common spatial resolution and differenced to obtain distributed elevation change. After filtering of outliers and gap filling using a local mean hypsometric method (60), we compute the mean elevation change within the glacier outlines and convert it to glacier mass balance (in meter of water equivalent) assuming a volume-to-mass conversion factor of 850 kg · m⁻³. We compute the uncertainty of geodetic mass balance by considering the SD of elevation change on stable terrain, multiple spatial correlation lengths, and the uncertainty associated with glacier outlines delineation and elevation change to mass change conversion (more details given in *SI Appendix*).

Model Calibration and Validation. The configuration and calibration of TOPKAPI-ETH for our catchment follow a similar sequential procedure to that of previous studies (25, 54, 61–63), using a maximum of in situ data to calibrate the process-specific parameters and validate the model. We run a point-based energy-balance model using on-glacier AWSon data for the period 2013 to 2016, and the modeled hourly melt rates are used to calibrate the ETI parameters (61, 63, 64) that are then validated against ablation stakes. The albedo-related parameters are calibrated against the albedo measured at AWSon, computed as the ratio of reflected and incoming shortwave radiation. Precipitation amounts at base station and vertical gradients are adjusted based on albedo measurements and geodetic mass balance of the period 2000 to 2016 and validated against a shallow ice core extracted from the accumulation zone. The 2016 discharge record is used to calibrate runoff routine parameters. Finally, the model is validated against geodetic mass balance and independent discharge records not used in the calibration process and fractional snow cover derived from MODIS imagery. More details on the calibration and validation procedure are given in *SI Appendix*, and the values of the parameters used are summarized in *SI Appendix, Table S2*. We perform a parametric sensitivity analysis and find that GMB and runoff are mostly sensitive to temperature-, albedo-, and precipitation-related parameters, but our results derived from a comparison between the two subperiods (Fig. 3) are not compromised by the parameter uncertainty (cf. *SI Appendix, section 6G*).

Attribution of Accelerated Mass Loss. An analysis of the cryospheric water balance was conducted to understand which components were most affected by the recent warming and caused the acceleration in glacier mass loss. This analysis compared the spring (March–April–May), monsoonal (June–July–August–September), and postmonsoon/winter (October–November–December–January–February) changes in icemelt, snowmelt, and snowfall between two periods (1975 to 1999 and 2000 to 2018). A change in snowfall ($\Delta Snowfall$) can result from two processes: 1) a change in precipitation amount and 2) a change in precipitation type. Both processes are simultaneous and assumptions are needed to quantify them separately. We compute the first process ($\Delta Snowfall_{\Delta precip}$) from the total precipitation change ($\Delta Precip$) assuming no change in the phase since the early period. Because the snowfall ratio was higher in the early period, this allows us to give a conservative estimation of the second term ($\Delta Snowfall_{\Delta phase}$). The formula used and the description of the remaining terms are given below:

$$\begin{aligned}\Delta Snowfall_{\Delta precip} &= \Delta Precip * r_{1975\ to\ 1999} \\ \Delta Snowfall_{\Delta phase} &= Precip_{2000\ to\ 2018} * (r_{2000\ to\ 2018} - r_{1975\ to\ 1999}) \\ \Delta Snowfall &= \Delta Snowfall_{\Delta precip} + \Delta Snowfall_{\Delta phase},\end{aligned}$$

where $P_{2000\ to\ 2018}$ is the mean precipitation of the recent period, and $r_{1975\ to\ 1999}$ and $r_{2000\ to\ 2018}$ are the mean snowfall to total precipitation ratios averaged over the early and the recent period, respectively. The computation of the uncertainty in $\Delta Snowfall_{\Delta phase}$ is described and discussed *SI Appendix, section 6F*. The relative contributions to total mass loss in the recent period (Fig. 3C) are computed as the net annual changes of each component leading to accelerated mass loss ($\Delta Icemelt$, $\Delta Snowmelt$, and $\Delta Snowfall_{\Delta phase}$) divided by their sum. The changes in snowfall attributed to precipitation change ($\Delta Snowfall_{\Delta precip}$) are not leading to more mass loss when aggregated annually and are therefore not included in the pie chart in Fig. 3 (cf. *SI Appendix, Fig. S21* for a complementary visualization of seasonal changes).

Data, Materials, and Software Availability. All input data, Matlab scripts, as well as data used for calibration and validation have been deposited in Zenodo at [10.5281/zenodo.6974319](https://zenodo.org/record/6974319) (65).

ACKNOWLEDGMENTS. This project received funding from the European Research Council under the European Union's Horizon 2020 research and innovation programme Grant 772751, RAVEN (Rapid mass losses of debris-covered glaciers in High Mountain Asia), and from the Swiss National Science Foundation (ASCENT Project 189890). Funding for the instrumentation of the Parlung catchment was provided by National Natural Science Foundation of China Projects 91647205 and 41961134035 and Newton Advanced Fellowship NA170325. The

scientific editor and reviewers are thanked for their insightful and constructive comments that have improved the quality of the manuscript.

Author affiliations: ^aMountain Hydrology and Mass Movements Unit, Swiss Federal Institute for Forest, Snow and Landscape Research (WSL), 8903 Birmensdorf, Switzerland; ^bInstitute of Environmental Engineering, ETH Zurich, 8093 Zurich, Switzerland; ^cBritish Antarctic Survey, Natural Environment Research Council, Cambridge, CB3 0ET, United Kingdom; ^dInstitute of Tibetan Plateau Research, Chinese Academy of Sciences, 100101 Beijing, China; ^eUniversity of Grenoble Alpes, CNRS, Research Institute for Sustainable Development (IRD), Institute of Environmental Geosciences (IGE), F-38000 Grenoble, France; ^fLaboratory of Hydraulics, Hydrology and Glaciology (VAW), ETH Zurich, 8093 Zurich, Switzerland; and ^gDepartment of Geography, Northumbria University, Newcastle, NE1 8ST, United Kingdom

1. D. Farinotti *et al.*, A consensus estimate for the ice thickness distribution of all glaciers on Earth. *Nat. Geosci.* **12**, 168–173 (2019).
2. W. W. Immerzeel *et al.*, Importance and vulnerability of the world's water towers. *Nature* **577**, 364–369 (2020).
3. A. Sakai, K. Fujita, Contrasting glacier responses to recent climate change in high-mountain Asia. *Sci. Rep.* **7**, 13717 (2017).
4. Y. Nie *et al.*, Glacial change and hydrological implications in the Himalaya and Karakoram. *Nat. Rev. Earth Environ.* **2**, 91–106 (2021).
5. H. Biemans *et al.*, Importance of snow and glacier meltwater for agriculture on the Indo-Gangetic Plain. *Nat. Sustain.* **2**, 594–601 (2019).
6. G. Voh, O. Korup, A. Walz, Hazard from Himalayan glacier lake outburst floods. *Proc. Natl. Acad. Sci. U.S.A.* **117**, 907–912 (2020).
7. T. Mölg, F. Maussion, D. Scherer, Mid-latitude westerlies as a driver of glacier variability in monsoonal High Asia. *Nat. Clim. Chang.* **4**, 68–73 (2014).
8. S. Li, T. Yao, W. Yang, W. Yu, M. Zhu, Glacier energy and mass balance in the inland Tibetan Plateau: Seasonal and interannual variability in relation to atmospheric changes. *J. Geophys. Res. Atmos.* **123**, 6390–6409 (2018).
9. T. Yao *et al.*, Different glacier status with atmospheric circulations in Tibetan Plateau and surroundings. *Nat. Clim. Chang.* **2**, 663–667 (2012).
10. R. Wang, S. Liu, D. Shangguan, V. Radić, Y. Zhang, Spatial heterogeneity in glacier mass-balance sensitivity across High Mountain Asia. *Water* **11**, 776 (2019).
11. P. Zhao, B. Wang, X. Zhou, Boreal summer continental monsoon rainfall and hydroclimate anomalies associated with the Asian-Pacific Oscillation. *Clim. Dyn.* **39**, 1197–1207 (2012).
12. T. Mölg, F. Maussion, W. Yang, D. Scherer, The footprint of Asian monsoon dynamics in the mass and energy balance of a Tibetan glacier. *Cryosphere* **6**, 1445–1461 (2012).
13. Y. Zhu, Y. F. Sang, D. Chen, B. Sivakumar, D. Li, Effects of the South Asian summer monsoon anomaly on interannual variations in precipitation over the South-Central Tibetan Plateau. *Environ. Res. Lett.* **15**, 124067 (2020).
14. F. Brun, E. Berthier, P. Wagnon, A. Käb, D. Treichler, A spatially resolved estimate of High Mountain Asia glacier mass balances, 2000–2016. *Nat. Geosci.* **10**, 668–673 (2017).
15. D. E. Shean *et al.*, A systematic, regional assessment of High Mountain Asia Glacier mass balance. *Front. Earth Sci.* **7**, 363 (2020).
16. R. Hugonnet *et al.*, Accelerated global glacier mass loss in the early twenty-first century. *Nature* **592**, 726–731 (2021).
17. B. Wu, Weakening of Indian summer monsoon in recent decades. *Adv. Atmos. Sci.* **22**, 21–29 (2005).
18. S. Ren *et al.*, Glacier mass balance in the Nyainqentanglha mountains between 2000 and 2017 retrieved from ZiYuan-3 stereo images and the SRTM DEM. *Remote Sens.* **12**, 864 (2020).
19. W. Yang *et al.*, Mass balance of a maritime glacier on the southeast Tibetan Plateau and its climatic sensitivity. *J. Geophys. Res. Atmos.* **118**, 9579–9594 (2013).
20. F. Maussion *et al.*, Precipitation seasonality and variability over the Tibetan Plateau as resolved by the high Asia reanalysis. *J. Clim.* **27**, 1910–1927 (2014).
21. Y. Shi, S. Liu, Estimation on the response of glaciers in China to the global warming in the 21st century. *Chin. Sci. Bull.* **45**, 668–672 (2000).
22. M. Zhu *et al.*, Differences in mass balance behavior for three glaciers from different climatic regions on the Tibetan Plateau. *Clim. Dyn.* **50**, 3457–3484 (2018).
23. T. Yao *et al.*, Recent third pole's rapid warming accompanies cryospheric melt and water cycle intensification and interactions between monsoon and environment: Multidisciplinary approach with observations, modeling, and analysis. *Bull. Am. Meteorol. Soc.* **100**, 423–444 (2019).
24. M. van Tiel, K. Stahl, D. Freudiger, J. Seibert, Glacio-hydrological model calibration and evaluation. *Adv. Rev.* **7**, e1483 (2020).
25. S. Ragettli *et al.*, Unraveling the hydrology of a Himalayan catchment through integration of high resolution in situ data and remote sensing with an advanced simulation model. *Adv. Water Resour.* **78**, 94–111 (2015).
26. A. Arndt, D. Scherer, C. Schneider, Atmosphere driven mass-balance sensitivity of Halji Glacier, Himalayas. *Atmosphere* **12**, 426 (2021).
27. H. Gao, X. He, B. Ye, J. Pu, Modeling the runoff and glacier mass balance in a small watershed on the Central Tibetan Plateau, China, from 1955 to 2008. *Hydrol. Processes* **26**, 1593–1603 (2012).
28. M. Sun, Z. Li, X. Yao, M. Zhang, S. Jin, Modeling the hydrological response to climate change in a glacierized high mountain region, northwest China. *J. Glaciol.* **61**, 127–136 (2015).
29. W. Yang, X. Guo, T. Yao, M. Zhu, Y. Wang, Recent accelerating mass loss of southeast Tibetan glaciers and the relationship with changes in macroscale atmospheric circulations. *Clim. Dyn.* **47**, 805–815 (2016).
30. K. Fujita, Y. Ageta, Effect of summer accumulation on glacier mass balance on the Tibetan Plateau revealed by mass-balance model. *J. Glaciol.* **46**, 244–252 (2000).
31. E. Miles *et al.*, Health and sustainability of glaciers in High Mountain Asia. *Nat. Commun.* **12**, 2868 (2021).
32. A. Saha, S. Ghosh, A. S. Sahana, E. P. Rao, Failure of CMIP5 climate models in simulating post-1950 decreasing trend of Indian monsoon. *Geophys. Res. Lett.* **41**, 7323–7330 (2014).
33. M. K. Roxy *et al.*, Drying of Indian subcontinent by rapid Indian Ocean warming and a weakening land-sea thermal gradient. *Nat. Commun.* **6**, 7423 (2015).
34. W. Zhang, T. Zhou, L. Zhang, Wetting and greening Tibetan Plateau in early summer in recent decades. *J. Geophys. Res. Atmos.* **122**, 5808–5822 (2017).
35. Y. Liu, H. Chen, G. Zhang, J. Sun, H. Wang, The advanced South Asian monsoon onset accelerates lake expansion over the Tibetan Plateau. *Sci. Bull. (Beijing)* **64**, 1486–1489 (2019).
36. M. S. Pervez, G. M. Henebry, Spatial and seasonal responses of precipitation in the Ganges and Brahmaputra river basins to ENSO and Indian Ocean dipole modes: Implications for flooding and drought. *Hazards Earth Syst. Sci.* **15**, 147–162 (2015).
37. S. Hu, T. Zhou, Skillful prediction of summer rainfall in the Tibetan Plateau on multiyear time scales. *Sci. Adv.* **7**, eabf9395 (2021).
38. I. Kadel, T. Yamazaki, T. Iwasaki, M. R. Abdillahi, Projection of future monsoon precipitation over the central Himalayas by CMIP5 models under warming scenarios. *Clim. Res.* **75**, 1–21 (2018).
39. M. W. Jury *et al.*, Climate projections for glacier change modelling over the Himalayas. *Int. J. Climatol.* **40**, 1738–1754 (2020).
40. Y. Li, Y. Chen, F. Wang, Y. He, Z. Li, Evaluation and projection of snowfall changes in High Mountain Asia based on NASA's NEX-GDDP high-resolution daily downscaled dataset. *Environ. Res. Lett.* **15**, 104040 (2020).
41. P. D. A. Kraaijenbrink, E. E. Stigter, T. Yao, W. W. Immerzeel, Climate change decisive for Asia's snow meltwater supply. *Nat. Clim. Chang.* **11**, 591–597 (2021).
42. J. Gabbi, M. Carenzo, F. Pellicciotti, A. Bauder, M. Funk, A comparison of empirical and physically based glacier surface melt models for long-term simulations of glacier response. *J. Glaciol.* **60**, 1199–1207 (2014).
43. G. Zheng *et al.*, Increasing risk of glacial lake outburst floods from future third pole deglaciation. *Nat. Clim. Chang.* **11**, 411–417 (2021).
44. X. Zhu Li, Z. Jun Chen, X. Chao Fan, Z. Jiang Cheng, Hydropower development situation and prospects in China. *Renew. Sustain. Energy Rev.* **82**, 232–239 (2018).
45. D. Finger, F. Pellicciotti, M. Konz, S. Rimkus, P. Burlando, The value of glacier mass balance, satellite snow cover images, and hourly discharge for improving the performance of a physically based distributed hydrological model. *Water Resour. Res.* **47**, W07519 (2011).
46. F. Pellicciotti, C. Buergi, W. W. Immerzeel, M. Konz, A. B. Shrestha, Challenges and uncertainties in hydrological modeling of remote Hindu Kush/Karakoram/Himalayan (HKH) Basins: Suggestions for calibration strategies. *Mt. Res. Dev.* **32**, 39–50 (2012).
47. J. Muñoz Sabater *et al.*, ERA5-Land: A state-of-the-art global reanalysis dataset for land applications. *Earth Syst. Sci. Data Discuss.* **2021**, 1–50 (2021).
48. J. He *et al.*, The first high-resolution meteorological forcing dataset for land process studies over China. *Sci. Data* **7**, 25 (2020).
49. D. C. Reicosky, L. J. Winkelman, J. M. Baker, D. G. Baker, Accuracy of hourly air temperatures calculated from daily minima and maxima. *Agric. For. Meteorol.* **46**, 193–209 (1989).
50. J. G. Corripio, Vectorial algebra algorithms for calculating terrain parameters from DEMs and solar radiation modelling in mountainous terrain. *Int. J. Geogr. Inf. Sci.* **17**, 1–23 (2003).
51. T. E. Shaw *et al.*, Distributed summer air temperatures across mountain glaciers in the south-east Tibetan Plateau: Temperature sensitivity and comparison with existing glacier datasets. *Cryosphere* **15**, 595–614 (2021).
52. D. B. Kattel, T. Yao, W. Yang, Y. Gao, L. Tian, Comparison of temperature lapse rates from the northern to the southern slopes of the Himalayas. *Int. J. Climatol.* **35**, 4431–4443 (2015).
53. W. Yang, T. Yao, M. Zhu, Y. Wang, Comparison of the meteorology and surface energy fluxes of debris-free and debris-covered glaciers in the southeastern Tibetan Plateau. *J. Glaciol.* **63**, 1090–1104 (2017).
54. F. Burger *et al.*, Interannual variability in glacier contribution to runoff from a high-elevation Andean catchment: Understanding the role of debris cover in glacier hydrology. *Hydrol. Processes* **33**, 214–229 (2019).
55. B. Ding *et al.*, Development of a water and enthalpy budget-based glacier mass balance model (WEB-GM) and its preliminary validation. *Water Resour. Res.* **53**, 3146–3178 (2017).
56. F. Pellicciotti *et al.*, An enhanced temperature-index glacier melt model including the shortwave radiation balance: Development and testing for Haut Glacier d'Arolla, Switzerland. *J. Glaciol.* **51**, 573–587 (2005).
57. B. W. Brock, I. C. Willis, M. J. Sharp, Measurement and parameterization of albedo variations at Haut Glacier d'Arolla, Switzerland. *J. Glaciol.* **46**, 675–688 (2000).
58. W. Yang *et al.*, Seasonal dynamics of a temperate Tibetan glacier revealed by high-resolution UAV photogrammetry and in situ measurements. *Remote Sens.* **12**, 2389 (2020).
59. M. Huss, G. Jouvett, D. Farinotti, A. Bauder, Future high-mountain hydrology: A new parameterization of glacier retreat. *Hydrol. Earth Syst. Sci.* **14**, 815–829 (2010).
60. R. McNabb, C. Nuth, A. Käb, L. Girod, Sensitivity of glacier volume change estimation to DEM void interpolation. *Cryosphere* **13**, 895–910 (2019).
61. A. Ayala *et al.*, Modelling the hydrological response of debris-free and debris-covered glaciers to present climatic conditions in the semiarid Andes of central Chile. *Hydrol. Processes* **30**, 4036–4058 (2016).
62. A. Ayala *et al.*, Glacier runoff variations since 1955 in the Maipo River basin, in the semiarid Andes of central Chile. *Cryosphere* **14**, 2005–2027 (2020).
63. T. E. Shaw *et al.*, The utility of optical satellite winter snow depths for initializing a glacio-hydrological model of a high-elevation, Andean catchment. *Water Resour. Res.* **56**, e2020WR027188 (2020).
64. A. Ayala, F. Pellicciotti, S. MacDonell, J. McPhee, P. Burlando, Patterns of glacier ablation across North-Central Chile: Identifying the limits of empirical melt models under sublimation-favorable conditions. *Water Resour. Res.* **53**, 5601–5625 (2017).
65. A. Jouberton *et al.*, Dataset - Warming-induced monsoon precipitation phase change intensifies glacier mass loss in the southeastern Tibetan Plateau. Zenodo. <https://zenodo.org/record/6974319>. Deposited 31 May 2021.